Article

Energetic and Electronic Structure Analysis of Intrinsic Defects in SnO

Kate G. Godinho, Aron Walsh, and Graeme W. Watson

J. Phys. Chem. C, **2009**, 113 (1), 439-448 • Publication Date (Web): 08 December 2008

Energetic and Electronic Structure Analysis of Intrinsic Defects in SnO_2

Kate G. Godinho, Aron Walsh, and Graeme W. Watson*

School of Chemistry, Trinity College Dublin, Dublin 2, Ireland

Received: September 1, 2008; Revised Manuscript Received: October 7, 2008

Empirically, intrinsic defects in SnO_2 are known to give rise to a net oxygen substoichiometry and n-type conductivity; however, the atomistic nature of the defects is unclear. Through first-principles density functional theory calculations, we present detailed analysis of both the formation energies and electronic properties of the most probable isolated defects and their clustered pairs. While stoichiometric Frenkel and Schottky defects are found to have a high energetic cost, oxygen vacancies, compensated through Sn reduction, are predicted to be the most abundant intrinsic defect under oxygen-poor conditions. These are likely to lead to conductivity through the mobility of electrons from Sn(II) to Sn(IV) sites. The formation of Sn interstitials is found to be higher in energy, under all charge states and chemical environments. Although oxygen interstitials have low formation energies under extreme oxygen-rich conditions, they relax to form peroxide ions (O_2^{2-}) with no possible mechanism for p-type conductivity.

Introduction

Transparent conducting oxides (TCOs) are solid-state oxides that combine the properties of optical transparency and electrical conductivity. In order for a material to be transparent, the band gap must be greater than the highest frequency of visible light, i.e., 3.1 eV.[1] Hence materials such as metals that are highly conductive normally do not transmit visible light, whereas highly transparent materials such as glasses usually behave as insulators. Conductivity in TCOs generally occurs due to the presence of native defects, which can be further enhanced through extrinsic aliovalent doping. These impurities introduce states into the band gap of the material causing p-type conduction if empty defect states occur near the valence band or n-type conduction if filled defect states occur near the conduction band. These defect levels must be shallow in order to enhance the conductivity without affecting the transparency. The majority of TCO materials occur with n-type conductivity (SnO_2, ZnO, In_2O_3), but some p-type TCOs such as $CuAlO_2$, $SrCu_2O_2$, and NiO are also known.[2,3] For practical use as transparent electrodes in devices such as solar cells, flat panel displays, and light emitting diodes, a TCO must have a resistivity of less than 10^{-3} Ω cm and over 80% transmittance in the visible range.[4] Indium tin oxide (ITO) is the current industrial standard material for transparent electrodes as thin films can be produced with resistivities of the order of 10^{-5} Ω cm. However, due to the expense and rarity of indium, alternatives need to be found. Tin dioxide is a promising such material, but its conductivity does not yet approach that of ITO.

SnO_2 crystallizes with the rutile structure, space group $P42/mnm$ (D_{4h}^{14}), in which each Sn(IV) ion sits at the center of a slightly distorted oxygen octahedron (Figure 1).[5] Sn also possesses a lower +2 oxidation state, with Sn(II) adopting distorted 4-fold coordination in the corresponding monoxide SnO.[6] In its stoichiometric form SnO_2 acts as an insulator, but in its oxygen-deficient form tin dioxide behaves as an n-type semiconductor with a band gap of 3.6 eV. Although the conductivity is thought to be due to intrinsic defect formation, the exact mechanism is not well understood. The bulk electronic structure has been investigated by a number of authors,[7–11] although the detailed defect electronic structure has not yet been studied. Oxygen deficiency may be caused either by oxygen vacancies or tin interstitials, with reduction of some Sn(IV) ions to Sn(II) as a possible charge compensation mechanism as suggested by the observation of a SnO phase in high-resolution transmission electron microscopy (HRTEM)[12] and fine structure emissions ascribed to Sn(II) in photoluminescence spectra.[13] Electronic conductivity could then occur due to the mobility of electrons from Sn(II) to Sn(IV) sites.[14,15]

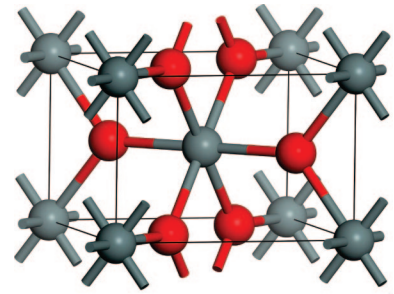

Figure 1. Unit cell of SnO_2. Red atoms are oxygen and gray atoms are tin.

Experimental data suggests that the cause of the nonstoichiometry in SnO_2 is oxygen vacancies rather than tin interstitials. The measurement of conductivity as a function of O_2 partial pressure has shown results consistent with the oxygen vacancy model.[16,17] Electron paramagnetic resonance (EPR) studies have identified a resonance at $g = 1.89$ associated with singly ionized oxygen vacancies ($V_O^\bullet$ in Kröger−Vink notation).[18–20] This resonance occurs after CO/Ar treatment of SnO_2, which results in the formation of $V_O^\bullet$ through the interaction of CO with surface oxygen to form CO_2 and neutral oxygen vacancies by the defect reaction $CO + O_O \rightarrow CO_2 + V_O^\times$. This forms a paramagnetic defect through the defect reaction $V_O^\times \rightarrow V_O^\bullet + e'$, producing an electron in the conduction band of Sn 5s character as evidenced in EPR by a resonance at $g = 1.99$ assigned to an unpaired electron on tin.[21] $V_O^\bullet$ is thought to transfer electrons onto tin ions to form $V_O^{\bullet\bullet}$ through the reaction $Sn_{Sn}^\times + 2V_O^\bullet \rightarrow Sn_{Sn}'' + 2V_O^{\bullet\bullet}$. Shallow donor levels for $V_O^\bullet/V_O^\times$ and $V_O^{\bullet\bullet}/V_O^\bullet$ have

* To whom correspondence should be addressed. Email: watsong@tcd.ie.

10.1021/jp807753t CCC: $40.75
Published on Web 12/08/2008

TABLE 1: Calculated Structural Parameters of SnO_2 Compared to Experimental Values[5]

	experimental	calculated (error)
a (Å)	4.740	4.834 (+2.0%)
c (Å)	3.188	3.244 (+1.8%)
u	0.3063	0.3066 (+0.1%)
Sn−O (Å)	4 × 2.05, 2 × 2.06	4 × 2.09, 2 × 2.10

been identified 0.03 and 0.15 eV below the conduction band minimum (CBM), respectively.[16,22] As these states lie quite close to the CBM, they will not cause a loss of transparency but will enhance the conductivity by introducing carrier electrons into the conduction band. Further evidence for the existence of these shallow states comes from cathodoluminescence studies which identified a band at 1.94 eV to result from a transition between a surface oxygen vacancy level at 1.4 eV above the valence band maximum (VBM) and a bulk shallow donor level at 0.15 eV below the CBM.[22]

There are few computational studies of defects in SnO_2 and these have concentrated mainly on energetics without analysis of the defect structure. Schottky and Frenkel defects have been studied using a force field approach. Freeman and Catlow[23] predicted the most stable defect to be the Schottky defect, whereas Hines et al. predicted it to be the oxygen Frenkel.[24] As neither of these defects result in a change in stoichiometry, they are not important in terms of conductivity. In a study of defect levels in SnO_2 using tight-binding Green's function calculations, the oxygen vacancy was found to form shallow donor levels.[25] The same shallow levels were later observed in a DFT study of charged defects.[26] However, contrary to the experimental evidence, the data from the latter study suggest that under oxygen-poor conditions $Sn_i^{\bullet\bullet\bullet\bullet}$ is the most stable defect rather than $V_O^{\bullet\bullet}$. As these are highly charged defects, they will not form in isolation as the crystal must be charge neutral overall. In addition, these charged defects do not provide any charge carriers for conductivity. They should thus be combined with some charge compensation mechanism such as Sn_{Sn}'' before their stability and effect on conductivity can be predicted. A later DFT study using a posteriori corrections to improve the description of the band gap contradicted these results and found oxygen vacancies to be the most stable intrinsic defect.[27] However, as oxygen vacancies were found to produce donor levels located deep in the band gap, the study concluded that they could not be responsible for the observed n-type conductivity of SnO_2. Instead, hydrogen impurities were proposed to be responsible for shallow donor levels observed experimentally and hence the conductivity. Neither of these DFT studies presented detailed analysis of electronic structure, so the exact structure of intrinsic defects has yet to be determined.

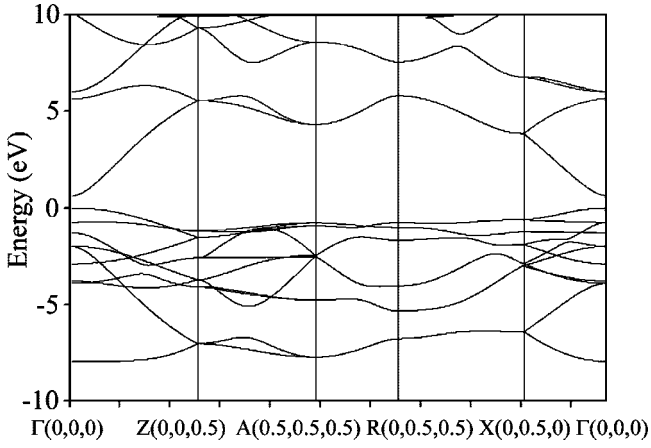

Figure 2. GGA band structure of SnO_2.

In this paper we present a comprehensive study of intrinsic defects in SnO_2. We initially discuss the defect energetics to identify the most stable defects. We will then discuss the geometry and electronic structure of a selection of these defects in order to understand the reasons behind their stability. As expected, we find that defects resulting in a net oxygen deficiency are favored; however, it is the oxygen vacancy and not the tin interstitial which has the lowest formation energy. These defects are facilitated by the ease in reducing Sn(IV) to Sn(II), in particular for the oxygen vacancy defect where the tin coordination environment is lowered. Conversely, the defects resulting in an oxygen excess (e.g., cation vacancies and oxygen interstitials) are higher in energy. Although oxygen interstitials are found to have low formation energies under extreme oxygen-rich conditions, they relax to give a peroxide ion structure (O_2^{2-}) which cannot produce free charge carriers to cause p-type conductivity. Our results therefore provide a microscopic understanding for the origin of substoichiometry in SnO_2.

Calculation Details

DFT as implemented in the Vienna Ab-Initio Simulation Package (VASP)[28,29] was used to calculate the equilibrium geometry and electronic structure. The Kohn−Sham[30] equations were solved self-consistently using the blocked Davidson diagonalization routine. The forces on the atoms were calculated using the Hellman−Feynman theorem and the atoms relaxed until the forces had converged to less than 0.01 eV/Å at constant volume. Generalized gradient (GGA) corrections were applied to the exchange-correlation functional within the implementation of Perdew, Burke, and Ernzerhof.[31]

A plane wave basis set was used to represent the wave functions with periodic boundary conditions applied in three dimensions to approximate the bulk solid. The projector augmented wave method[32] was used to represent the interaction between the core electrons (Sn:[Kr], O:[He]) and valence electrons, as it approaches the accuracy of an all-electron calculation. The plane wave cutoff energy (500 eV) and k-point density, obtained using the Monkhorst−Pack[33] method, were both checked for convergence to within 0.01 eV/cation.

A supercell expansion of 3 × 3 × 4 (216 atoms) was used for defect calculations, with a k-point grid of 2 × 2 × 2. Defect calculations were carried out by placing each defect in the supercell which is then repeated infinitely in space so that a periodic lattice of defects is formed. The energy convergence with supercell size was tested, as the cell must be large enough in order to avoid defect−defect interactions that would not occur in a real crystalline system in the dilute limit. For charged defects, a uniform background charge is assumed in order to maintain overall charge neutrality. Although the defect formation energy of these individual charged defects is dependent on the Fermi energy,[26] here we combine charged defects to form charge neutral species which are independent of Fermi level. The defect formation energies $E_f(D)$ were calculated using

$$E_f(D) = E_{tot}(D) - E_{tot}(SnO_2) + \frac{1}{2}n_O E(O_2) + n_{Sn}E(\alpha\text{-Sn}) + n_O\mu_O + n_{Sn}\mu_{Sn} \quad (1)$$

where $E_{tot}(D)$ is the total energy for the supercell containing the defect D and $E_{tot}(SnO_2)$, $E(O_2)$, and $E(\alpha\text{-Sn})$ are the total energies of the pure SnO_2 supercell, the O_2 molecule, and of a Sn atom in α-Sn respectively. n_O and n_{Sn} are the number of

oxygen and tin atoms removed from the system and μ_O and μ_{Sn} are the chemical potentials of oxygen and tin, respectively. For example, the creation of an oxygen vacancy can be represented in Kröger−Vink notation as

$$O_O^{\times} \rightarrow V_O^{\bullet\bullet} + 2e' + \frac{1}{2}O_2 \quad (2)$$

For this defect $n_O = +1$ and $n_{Sn} = 0$ so only the oxygen terms are included in eq 1. The total energy of the oxygen molecule is calculated as −9.85 eV. However, as GGA is known to overstabilize the O_2 molecule,[34] we have calculated that for the PBE functional used, a correction of +1.4 eV to its total energy is required. Thus, for the formation energy of an oxygen vacancy, a correction of +0.7 eV is applied. The isolated oxygen vacancy ($V_O^{\bullet\bullet}$) is calculated with the two electrons removed from the cell. The compensating defect is a two-electron reduction of one Sn(IV) atom to Sn(II) through the defect reaction:

$$Sn_{Sn}^{\times} + 2e' \rightarrow Sn_{Sn}'' \quad (3)$$

As in this case no ions have been added/removed from the system, both n_O and n_{Sn} in eq 1 are zero. The combined neutral defect reaction is calculated from

$$Sn_{Sn}^{\times} + O_O^{\times} \rightarrow V_O^{\bullet\bullet} + Sn_{Sn}'' + \frac{1}{2}O_2 \quad (4)$$

Alternatively, if we insert a tin atom into the system to form a tin interstitial, the corresponding defect reaction is

$$V_i^{\times} + Sn(s) \rightarrow Sn_i^{\bullet\bullet\bullet\bullet} + 4e' \quad (5)$$

Here, $n_O = 0$ and $n_{Sn} = -1$ so that the oxygen terms disappear from eq 1. The isolated interstitial ($Sn_i^{\bullet\bullet\bullet\bullet}$) is calculated with the four electrons removed from the cell. The compensating defect is the reduction of two Sn(IV) ions to Sn(II) as in eq 3 so that the combined neutral defect reaction is calculated from

$$2Sn_{Sn}^{\times} + Sn(s) + V_i^{\times} \rightarrow Sn_i^{\bullet\bullet\bullet\bullet} + 2Sn_{Sn}'' \quad (6)$$

Variation of the chemical potentials in eq 1 is equivalent to varying the oxygen partial pressure experimentally. The oxygen-rich limit occurs when μ_O is equal to the chemical potential of oxygen in O_2 (0 eV). The oxygen-poor limit is defined when μ_O equals the energy of decomposition of SnO_2 ($SnO_2 \rightarrow SnO + {}^1/_2O_2$) calculated as −3.09 eV compared to a value of −3.08 eV experimentally.[35] The full constraint is thus $-3.09\ eV < \mu_O < 0\ eV$. μ_{Sn} is determined by the formation energy of SnO_2, which is calculated as −6.39 eV compared to −5.98 eV experimentally.[35] Hence μ_{Sn} can be calculated using $\mu_{Sn} = \Delta H_{SnO_2} - 2\mu_O$ giving a range of $-6.39\ eV < \mu_{Sn} < -0.20\ eV$.

Bulk Electronic Structure

Full geometry and volume optimizations were performed on the initial experimental structure[5] with the equilibrium volume obtained from a fit to the Murnaghan equation of state.[36] The calculated lattice parameters and bond lengths are increased from their experimental values by about 2%, as expected for GGA calculations (Table 1). Bader charge analysis was performed using the code developed by Henkelman et al.[37] and shows the tin atoms to have a charge of 2.52 and the oxygen atoms to have a charge of −1.26. This indicates a high degree of covalent character in the bonding as seen in previous studies of SnO_2[38,39] and the corresponding monoxide SnO.[6,40,41]

The band structure of the bulk material is shown in Figure 2 and exhibits similar topology to previous calculations.[7,8,10,11] The calculated band gap is 0.6 eV, as compared to the experimental value of 3.6 eV. This is not unexpected as DFT is known to greatly underestimate the band gaps of metal oxides, despite the fact that the ground-state properties are well described.[42] A direct band gap at Γ can be seen, consistent with optical measurements.[43] A large dispersion in the lowest lying conduction band at Γ of approximately 5 eV can also be observed, consistent with previous calculations. This has been suggested to be one of the important band structure features of a good transparent conducting oxide as it limits optical absorbance in the visible and infrared regions of the spectrum, and provides a light effective electron mass for carrier transport. [44]

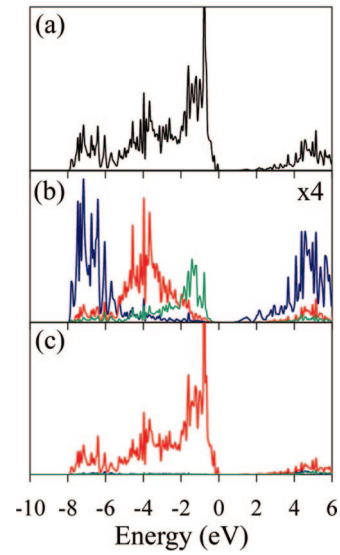

Figure 3. Electronic density of states (EDOS) of bulk SnO_2; blue lines represent s states, red are p states, and green are d states. Total EDOS (a) and partial EDOS for Sn (b) and O (c).

The electronic density of states (EDOS) is shown in Figure 3. The atomic projections were calculated with sphere radii of 1.50 Å for Sn and 1.32 Å for O. These radii were determined from consideration of the valence electron density around each ion and electron counting. Our EDOS compare well with previous calculations[7,9,39,45] and photoemission results.[39,46,47] The valence band (VB) is mainly made up of O 2p states. A significant density of Sn 5s states is seen in the valence band between −8 and −6 eV. Sn 5p states contribute to the VB from −6 to −2 eV. In the upper part of the VB from −5 to −1 eV, there is a slight contribution from Sn 4d states due to a small amount of mixing between the Sn 4d states and O 2p states in the lower VB at −21 eV (not shown here). This has been previously reported in other calculations,[7,38] and it was shown by crystal orbital overlap population (COOP) to be due to antibonding Sn 4d−O 2p interactions. The conduction band is of mainly Sn 5*s* character, with some Sn 5p, O 2s, and O 2p contributions.

Defect Formation Energies

We have considered a series of charge neutral intrinsic defects in SnO_2. These can be divided into stoichiometric defects, which do not result in a change in stoichiometry and will not therefore generate charge carriers, and the formation of nonstoichiometric defects which may contribute to conductivity in SnO_2.

We have introduced a number of isolated defects into the supercell in the indicated formal charge states. Tin and oxygen vacancies and interstitials were inserted, with the interstitials being placed in both tetrahedral and octahedral sites. Charge-neutral combinations of these defects were then considered with

TABLE 2: Defect Formation Energies of Neutral Combinations of Defects in SnO_2 Calculated from Isolated Defects and Defect Clusters. O-Rich Corresponds to $\mu_O = 0$ eV and O-Poor Corresponds to $\mu_O = -3.09$ eV

stoichiometric	isolated	cluster		
V_{Sn}'''' + $Sn_i^{••••}$ − oct	9.59	−		
V_{Sn}'''' + $Sn_i^{••••}$ − tet	9.80	−		
$V_O^{••}$ + O_i''	7.00	6.48		
V_{Sn}'''' + $2V_O^{••}$	11.01	6.48		
	O-poor		O-rich	
oxygen-deficient	isolated	cluster	isolated	cluster
$V_O^{••}$ + Sn_{Sn}''	2.14	1.45	5.24	4.54
$Sn_i^{••••}$ − oct + $2Sn_{Sn}''$	2.85	3.93	9.04	10.12
$Sn_i^{••••}$ − tet + $2Sn_{Sn}''$	3.07	3.73	9.26	9.92
$Sn_i^{••}$ − oct + Sn_{Sn}''	2.53	3.93	8.72	10.12
$Sn_i^{••}$ − tet + Sn_{Sn}''	2.84	3.73	9.03	9.92
$(Sn_i + V_O)^×$	−	3.70	−	12.98
oxygen-excess	isolated	cluster	isolated	cluster
V_{Sn}'''' + $4h^•$	14.09	12.13	7.90	5.94
O_i'' − tet + $2h^•$	8.54	5.11	5.44	2.02
O_i'' − oct + $2h^•$	8.54	5.41	5.44	2.32

their formation energies calculated from those of the individual charged defects. Calculations of neutral defect clusters formed by combining the formally charged defects in the same supercell were also performed so that the binding energy can be obtained from the difference in energy. We include a defect cluster composed of an oxygen vacancy and a tin interstitial $(Sn_i + V_O)^×$ as this defect was suggested to be the cause of oxygen deficiency in a previous DFT study.[26] The resulting defect formation energies are listed in Table 2 using Kröger−Vink notation to describe the defects. The tabulated defects are those inserted into the system and may relax to give different structures which will be discussed in more detail later.

The stoichiometric defects all have high formation energies which is important as it limits the formation of nonconducting defects. When the component charged defects are isolated, the anion Frenkel ($V_O^{••} + O_i''$) is the most stable stoichiometric defect. As tin interstitials were inserted into both octahedral and tetrahedral sites, two possible configurations for the cation Frenkel defect ($V_{Sn}'''' + Sn_i^{••••}$) resulted, with the octahedral configuration being lower in energy. Comparing our formation energies for isolated defects with previous forcefield calculations, Freeman and Catlow[23] calculated energies of 5.19, 5.54, and 9.63 eV for the Schottky ($V_{Sn}'''' + 2V_O^{••}$), anion Frenkel and cation Frenkel defects, respectively. Their calculated energy for the Schottky defect is much lower than our value. However, a later study by Hines et al.[24] using an improved potential model calculated energies of 11.32 and 7.99 eV for the Schottky and anion Frenkel defects, which are in better agreement with our results. Clustering the defects reduces their formation energies with the anion Frenkel and the Schottky defect clusters having identical formation energies. (The formation energy of the V_{Sn}'''' + $Sn_i^{••••}$ defect cluster is not shown as the interstitial recombined with the vacancy upon relaxation.) However, the formation energies are still high and nonstoichiometric defects are likely to dominate the defect structure.

It is found that the most stable nonstoichiometric defect is dependent on the oxygen partial pressure. Under oxygen-poor conditions, defects which cause oxygen excess $V_{Sn}'''' + 4h^•$ and $O_i'' + 2h^•$ have high formation energies and thus defects which cause oxygen deficiency will dominate under these conditions. The most stable defect is found to be $V_O^{••} + Sn_{Sn}''$. The binding energy of this defect is −0.69 eV, suggesting an enhanced stability when the defects occur in close proximity that arises from attractive Coulomb interactions. This result is in disagreement with the conclusions of Kilic and Zunger[26] who suggested that $Sn_i^{••••}$ is the most stable charged defect, indicating a tin interstitial dominated mechanism of nonstoichiometry. They concluded that a $(Sn_i + V_O)^×$ complex would be responsible for oxygen deficiency in SnO_2 due to a high energy of attraction between V_O and Sn_i. As the two component defects both normally occur in positive charge states, the exact nature of the defect suggested is unclear. It was proposed that the interstitial occurs in the +2 charge state but no charge compensation mechanism was suggested. However, our results show this defect to be much higher in energy than $V_O^{••} + Sn_{Sn}''$. If we examine the other possible combinations of defect involving tin interstitials ($Sn_i^{••••} + 2Sn_{Sn}''$ and $Sn_i^{••} + Sn_{Sn}''$), it can be seen that they have higher formation energies than $V_O^{••}$ + Sn_{Sn}'' and hence are less likely to form. Although tin interstitial formation may contribute to the overall nonstoichiometry, the dominant mechanism of oxygen deficiency will be oxygen vacancy formation.

Comparing the isolated energies to the clustered calculations shows that for most defects, clustering lowers the energy. However, the tin interstitial combinations show unusual behavior as the isolated formation energies are lower than the cluster calculations. The geometry of these defects will be examined later to investigate this discrepancy.

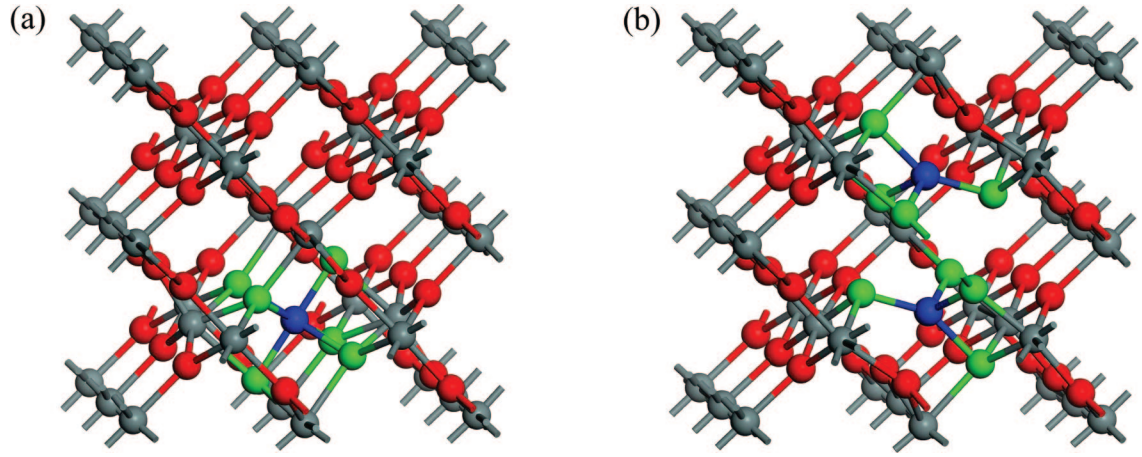

Figure 4. Local structure around tin interstitial defects in SnO_2: (a) $Sn_i^{••••}$–oct and $Sn_i^{••}$–oct and (b) $Sn_i^{••••}$–tet and $Sn_i^{••}$tet. Blue atoms indicate interstitials and green indicate nearest-neighbor oxygen atoms.

TABLE 3: Calculated Bader Charges for $Sn_i^{••••}$ and $Sn_i^{••}$ Inserted into Octahedral and Tetrahedral Environments in SnO_2[a]

	Sn_i	Sn_{av}	Sn_{tot}
SnO_2	−	2.52	181.49
SnO	−	1.25	−
$Sn_i^{••••}$−oct	2.35	2.52	183.74
$Sn_i^{••}$−oct	2.33	2.51	182.53
$Sn_i^{••••}$−tet	2.36, 2.34	2.52	183.81
$Sn_i^{••}$−tet	2.33, 2.32	2.51	182.54

[a] Sn_{av} and Sn_{tot} are the average and total Sn charge in each defective supercell.

Under oxygen-rich conditions, defects which cause oxygen deficiency increase in energy while defects which cause oxygen excess are lower in energy. The most stable nonstoichiometric defect under these conditions is the $O_i'' + 2h^•$ defect cluster. The formation energy of this defect differs depending on whether the interstitial is inserted into a tetrahedral or octahedral site with the tetrahedral defect being lower in energy by 0.30 eV. As the $O_i'' -$ tet $+ 2h^•$ defect cluster has a binding energy of −3.43 eV, there is clearly a large stabilization when the interstitial and the oxygen holes are considered together. We will examine the detailed geometry and electronic structure later to investigate the reasons behind this stabilization. Although the formation energy of $V_{Sn}'''' + 4h^•$ reduces under oxygen-rich conditions, it is still considerably higher than that of the oxygen interstitial. The reason for this is the high formation energy of oxygen holes. Formation of a hole requires an electron to be removed from the O 2p valence band which is highly unfavorable energetically due to the high electronegativity of oxygen. This contributes to the preference for substoichiometric defects ($SnO_{2-\delta}$). As V_{Sn}'''' is compensated by four oxygen holes in the valence band, its formation energy is high and it is unlikely to form.

Structure of Tin Interstitials

Tin interstitials inserted into tetrahedral and octahedral sites were found to relax to different equilibrium geometries. Very little deviation in structure was seen between the +2 and +4 charge states. The octahedral interstitials insert into the center of an oxygen octahedron with two Sn−O bond lengths of 2.00 Å and four of 2.13 Å (Figure 4a). The tin coordination is similar to that of Sn(IV) in bulk SnO_2. The tetrahedral interstitials both relax to give split interstitial structures in which the interstitial tin displaces a lattice tin to form two tetrahedral interstitials around a vacant lattice site (Figure 4b). $Sn_i^{••••}$−tet forms interstitials 3.73 Å apart with Sn−O bond lengths of 2 × 2.02, 2.05 and 1.96 Å, whereas $Sn_i^{••}$−tet forms two tetrahedral interstitials, 3.69 Å apart, with similar Sn−O bond lengths. Although the coordination of the tetrahedral interstitials is similar to that in SnO, the bond lengths are significantly shorter than those calculated for SnO (2.26 Å)[40,41] suggesting that the interstitials may not be in a +2 charge state.

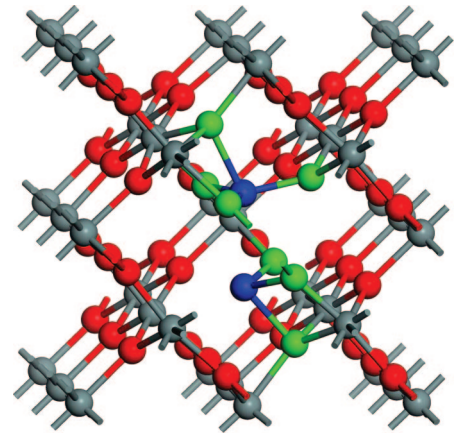

Figure 6. Local structure of the neutral defect cluster of an oxygen vacancy and tin interstitial ($(V_O + Sn_i)^×$) in SnO_2. Blue atoms are interstitials and green are nearest-neighbor oxygen atoms.

The Bader charges in Table 3 indicate all interstitials to be in the same charge state. Although the charge is lower than that of Sn in bulk SnO_2, in no case does it approach that of Sn in SnO (1.25). Given the small change in charge involved, the indication is that these are all Sn(IV) interstitials. This suggests that $Sn_i^{••••}$−oct is an accurate description of the defect whereas $Sn_i^{••••}$−tet in fact relaxes to give $2Sn_i^{••••} + V_{Sn}''''$. Regarding the inserted Sn(II) interstitials, as the interstitials relax to a +4 charge state, a charge-compensation mechanism must exist so that the overall charge is +2. As the average tin charge in the +2 system is lower than that in the +4 system, charge compensation is likely to be achieved by a tin reduction. The difference in total Sn charge between $Sn_i^{••••}$−oct and $Sn_i^{••}$−oct is 1.22 indicating an overall reduction of a single tin ion in the +2 system to Sn(II) (Sn_{Sn}''). Similarly, comparing the total Sn charge for $Sn_i^{••••}$−tet and $Sn_i^{••}$−tet shows a difference of 1.16 also suggesting the presence of a Sn reduction in the $Sn_i^{••}$−tet defect. The octahedral defect shows a slightly greater reduction

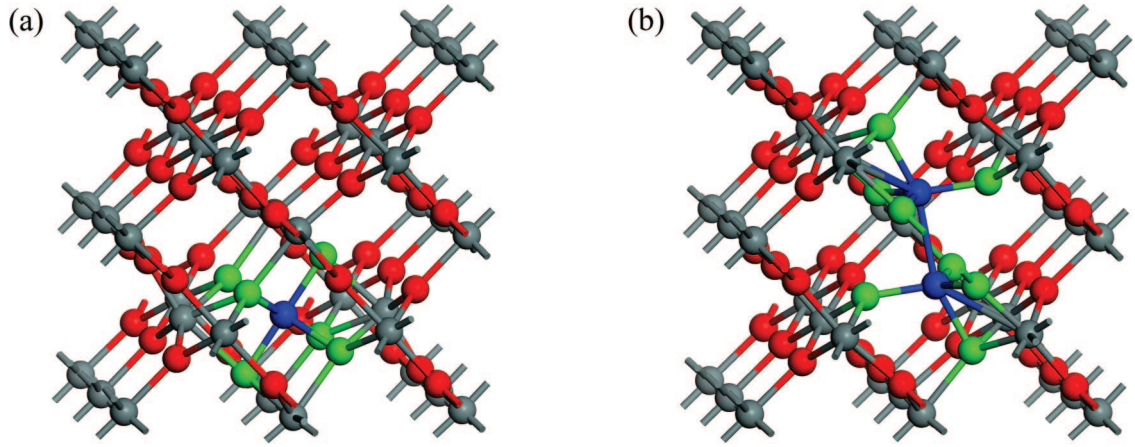

Figure 5. Local structure around tin interstitial defect clusters in SnO_2: (a) $Sn_i^{••••} -$ oct $+ 2Sn_{Sn}''$ and $Sn_i^{••} -$ oct $+ Sn_{Sn}''$; (b) $Sn_i^{••••} -$ tet $+ 2Sn_{Sn}''$ and $Sn_i^{••} -$ tet $+ Sn_{Sn}''$. Blue atoms are interstitials and green are nearest-neighbor oxygen atoms.

TABLE 4: Bader Charges for Tin Interstitial Clusters in SnO_2[a]

	Sn_i	Sn_{av}	Sn_{tot}
$Sn_i^{\bullet\bullet\bullet\bullet}$ − oct + $2Sn''_{Sn}$	2.30	2.50	181.27
$Sn_i^{\bullet\bullet\bullet\bullet}$ − tet + $2Sn''_{Sn}$	2 × 1.87	2.50	181.46
$(V_O + Sn_i)^{\times}$	1.75, 1.23	2.50	172.67

[a] Sn_i, Sn_{av}, and Sn_{tot} are the interstitial, average, and total tin charges.

TABLE 5: Bader Charges for $V_O^{\bullet\bullet} + Sn''_{Sn}$ in SnO_2[a]

	Sn_{nn}	Sn_{av}	Sn_{tot}
bulk	−	2.52	181.49
Sn''_{Sn}	−	2.50	180.08
$V_O^{\bullet\bullet}$	2 × 2.40, 2.41	2.52	181.30
$V_O^{\bullet\bullet} + Sn''_{Sn}$	2 × 2.27, 2.33	2.51	180.04

[a] Sn_{nn} are the charges on the tin ions neighboring the defect; Sn_{av} and Sn_{tot} are the average and total Sn charges in each supercell.

on the six tin ions neighboring the interstitial; however, this accounts for a total reduction in charge of only 0.24*e*. The remaining charge is delocalized over all tin ions in the system. $Sn_i^{\bullet\bullet}$−tet likewise shows a delocalized reduction. The observed delocalization is not unexpected as DFT is known to exaggerate the delocalization of defect states due to the self-interaction error.[48–50] Hence the inserted $Sn_i^{\bullet\bullet}$−oct defect relaxes to $Sn_i^{\bullet\bullet\bullet\bullet} + Sn''_{Sn}$ while the inserted $Sn_i^{\bullet\bullet}$−tet defect relaxes to $2Sn_i^{\bullet\bullet\bullet\bullet} + V''''_{Sn} + Sn''_{Sn}$.

The structures of the charge-neutral defect clusters, $Sn_i^{\bullet\bullet\bullet\bullet} + 2Sn''_{Sn}$ and $Sn_i^{\bullet\bullet} + Sn''_{Sn}$, are shown in Figure 5. As both of these defect clusters have the same number of electrons, both relax to give the same structure; however, different structures are obtained if the interstitial is inserted into an octahedral or tetrahedral site. The octahedral cluster has a similar geometry to that found for the isolated octahedral interstitials above, indicating it to be in a similar charge state. The tetrahedral cluster forms two tetrahedrally coordinated tin interstitials with a distance of 2.65 Å between them. This is structurally similar to the tetrahedral interstitials above except for a shorter Sn−Sn distance which may be an indication of a change in charge state. The $(V_O + Sn_i)^{\times}$ cluster suggested by Kilic and Zunger[26] exhibits a geometrically similar structure to that of the isolated tetrahedral interstitials (Figure 6). The interstitial displaces a lattice tin atom to form a split interstitial structure where the inserted interstitial coordinates to three tin ions while the displaced tin ion is tetrahedrally coordinated. Two other tin ions have lost coordination due to the creation of an oxygen vacancy.

The Bader charges for the tetrahedral and octahedral clusters are shown in Table 4. The octahedral interstitial has a similar charge to that found for the isolated interstitials above, indicating that it is most likely $Sn_i^{\bullet\bullet\bullet\bullet}$ with charge compensation achieved through a four-electron delocalized reduction on the tin atoms so that the overall defect is $Sn_i^{\bullet\bullet\bullet\bullet} + 2Sn''_{Sn}$. However, in the tetrahedral cluster the two interstitial tin atoms each possess a Bader charge of 1.87, intermediate between that of Sn(II) (1.25) and that of Sn(IV) (2.52). This indicates that the interstitials may be in an unusual intermediate +3 charge state. Charge compensation is again accomplished through a delocalized tin reduction. This gives rise to the overall defect structure of 2 $Sn_i^{\bullet\bullet\bullet} + V'''_{Sn} + Sn''_{Sn}$.

Bader analysis of the $(V_O + Sn_i)^{\times}$ defect cluster indicates the tetrahedral tin ion to have a charge of 1.75, while the 3-coordinate tin has a charge of 1.23. Two other tin ions neighboring the oxygen vacancy have lost coordination and have Bader charges of 2.23. The indication is that the 3-coordinate tin is in a +2 charge state while the tetrahedral tin is in a +3 charge state. Charge compensation is achieved through a 3-electron-reduction delocalized over the remaining tin atoms,

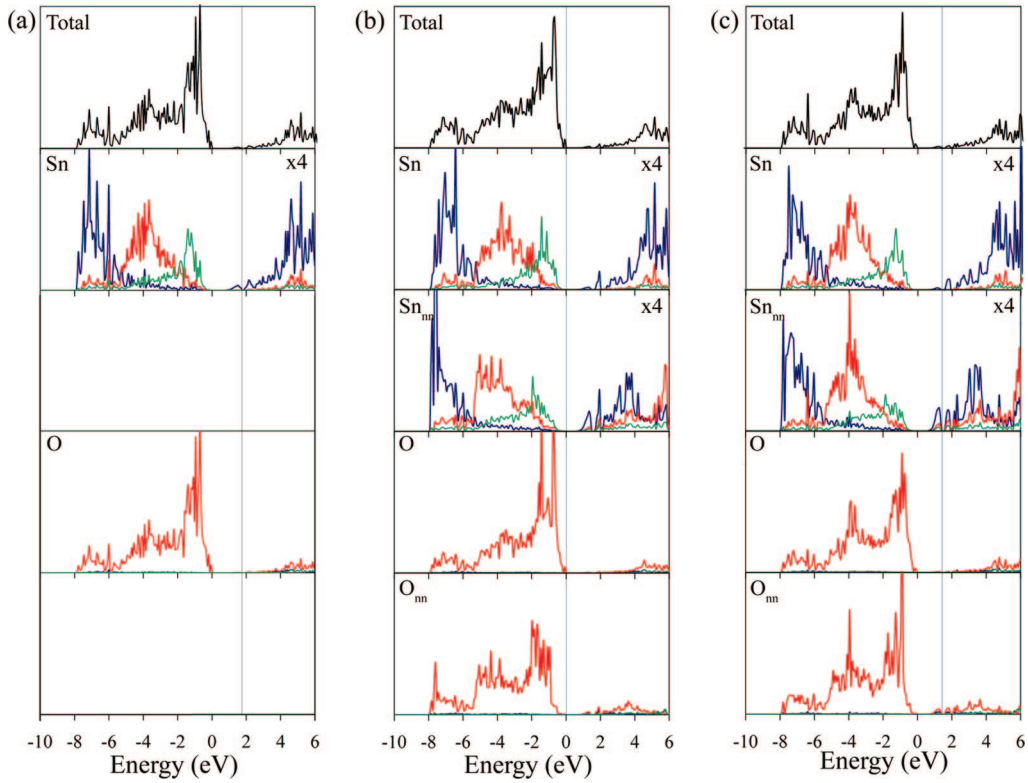

Figure 7. Total and partial electronic density of states for (a) Sn''_{Sn}, (b) $V_O^{\bullet\bullet}$, and (c) $V_O^{\bullet\bullet} + Sn''_{Sn}$ in SnO_2. Sn_{nn} and O_{nn} are tin and oxygen atoms neighboring the vacancy. Gray lines indicate position of highest occupied state. Blue lines are s, red are p, and green are d states.

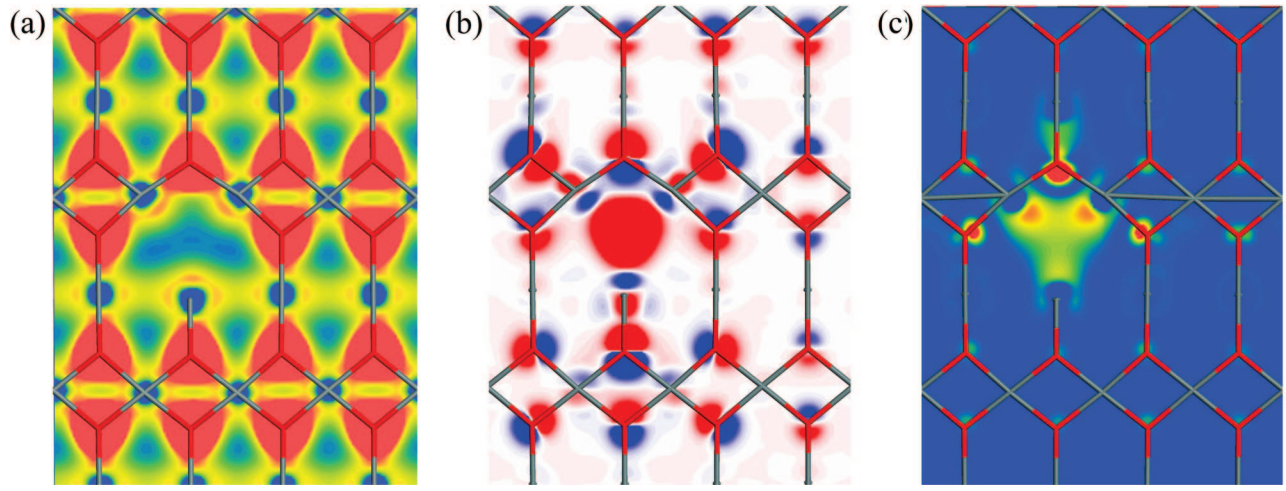

Figure 8. Charge density plots for $V_O^{\bullet\bullet} + Sn_{Sn}''$ in SnO_2. (a) Partial charge density from −10 eV to the defect state at contour levels from 0 (blue) to 0.3 e/Å^3 (red). (b) Charge density difference between valence band of bulk and defective cell at contour levels between −0.1 (red) and 0.1 e/Å^3 (blue). (c) Partial charge density of defect state at contour levels between 0 (blue) and 0.05 e/Å^3 (red).

with the 5-fold coordinate tin ions neighboring the vacancy having a greater tendency to reduce. This suggests that the defect is most closely described by $Sn_i^{\bullet\bullet} + Sn_i^{\bullet\bullet\bullet\bullet} + V_O^{\bullet\bullet} + V_{Sn}'''' + Sn_{Sn}'''$.

Electronic Structure of O-Poor Defects: Oxygen Vacancies

At low oxygen partial pressure, the most stable defect is $V_O^{\bullet\bullet}$ charge compensated by the reduction of a Sn(IV) ion to Sn(II) (Sn_{Sn}''). In the neutral defect cluster ($V_O^{\bullet\bullet} + Sn_{Sn}''$), formation of the oxygen vacancy leads to the loss of coordination of three neighboring tin ions and their relaxation away from the vacancy (two by 0.16 Å and one by 0.19 Å). In the isolated vacancy ($V_O^{\bullet\bullet}$) these tin atoms show a greater relaxation away from the vacancy (two by 0.26 and one by 0.25 Å) due to greater Coulombic repulsion between the tin ions.

The Bader charges for $V_O^{\bullet\bullet}$, Sn_{Sn}'' and their defect cluster are shown in Table 5. Sn_{Sn}'' occurs as a delocalized reduction rather than localizing on a single tin atom. This can be seen from the decrease in average tin charge from 2.52 in bulk tin dioxide to 2.50 in the defective supercell. The difference between total Sn charge in the bulk and defect cells for Sn_{Sn}'' is 1.41 which is indicative of a reduction to Sn(II) overall (Bader charge of 1.25). For $V_O^{\bullet\bullet}$ the average tin charge is the same as pure SnO_2; however, a slight reduction in charge on the three tin ions neighboring the vacancy is observed. It is likely that the change in electron density occurs as a result of the reduction in coordination of these tin ions from 6- to 5-fold coordinate. For $V_O^{\bullet\bullet} + Sn_{Sn}''$, there is a larger loss in charge on these three tin ions compared to the isolated vacancy, accounting for a total of 0.34*e* of the reduction. The remaining excess charge is delocalized over all tin ions in the system shown by the difference of 1.26 in total tin charge between the isolated vacancy and the combined defect.

The electronic density of states (EDOS) for both the isolated and combined defects is shown in Figure 7 with the valence band maximum at 0 eV. The bottom of the Sn 5s conduction band is occupied by $2e^-$ for both Sn_{Sn}'' and $V_O^{\bullet\bullet} + Sn_{Sn}''$. The EDOS for Sn_{Sn}'' is similar to that of bulk SnO_2 except for the occupation of states at the CBM. There are no apparent defect states in its DOS. However, as the tin reduction is fully delocalized this is not unexpected.

The EDOS for $V_O^{\bullet\bullet}$ shows an empty state split off from the CBM by 0.3 eV which is a mixture of Sn 5s character from the tin ions neighboring the vacancy and of O 2p character from oxygen ions close to the defect. For $V_O^{\bullet\bullet} + Sn_{Sn}''$, this state becomes filled by the extra $2e^-$ from the tin reduction. The location of this defect state agrees qualitatively with experimental evidence which places donor levels for oxygen vacancies 0.03−0.15 eV below the CBM.[16,22] Similar states of Sn 5s character have been observed on reduced SnO_2 surfaces by resonant photoemission spectroscopy due to the reduction of Sn(IV) ions neighboring oxygen vacancies to Sn(II).[47]

Charge density maps for $V_O^{\bullet\bullet} + Sn_{Sn}''$ are shown in Figure 8. The valence band partial charge density from −10 eV up to

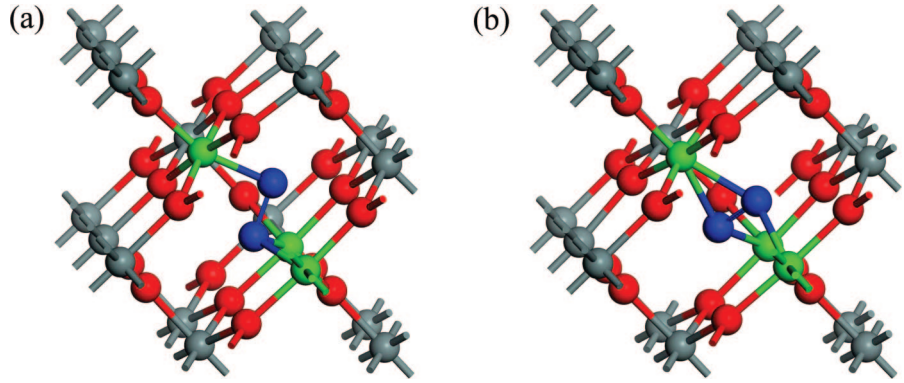

Figure 9. Local structure around $O_i'' + 2h^{\bullet}$ defect clusters in SnO_2. (a) Structure of interstitial inserted into octahedral site. (b) Structure of interstitial inserted into tetrahedral site. Blue atoms are peroxide ion and green atoms are neighboring Sn atoms.

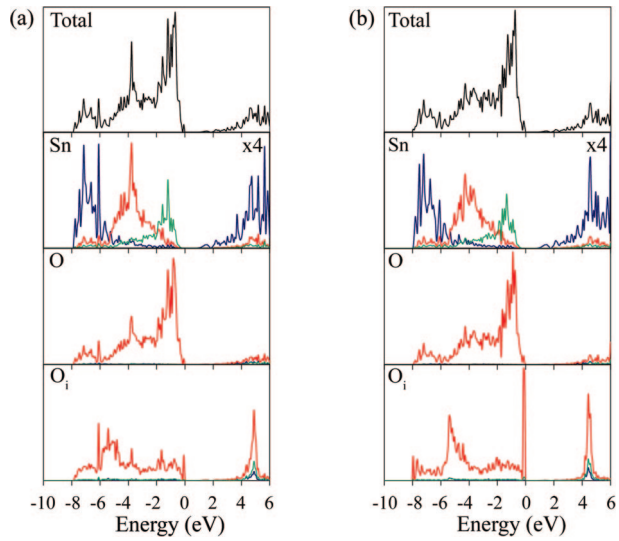

Figure 10. Electronic density of states for (a) $(O_2)_O^{\times}$−oct and (b) $(O_2)_O^{\times}$−tet in SnO_2. Blue lines are s states, red are p states, and green are d states.

TABLE 6: Bond Lengths and Bader Charges for Oxygen Interstitials in SnO_2[a]

	O−O (Å)	O_i	Sn_{av}	Sn_{tot}
O_i''	1.51	−0.69, −0.70	2.50	179.99
O_i'' − oct + 2h$^{\bullet}$	1.49	−0.71, −0.62	2.52	181.41
O_i'' − tet + 2h$^{\bullet}$	1.51	−0.70, −0.68	2.52	181.23

[a] O_i is the oxygen interstitial charge, Sn_{av} is the average Sn charge, and Sn_{tot} is the total Sn charge in the defective cell.

the defect state (Figure 8a) shows most of the density to be on the oxygen atoms with some spherical 5s character on Sn atoms consistent with the low-energy s states seen in the EDOS. The three Sn atoms surrounding the vacancy show lone-pair-like density consistent with the partial reduction indicated by Bader analysis. The charge density difference between the valence band of the defective and nondefective cells (Figure 8b) shows an increase in electron density on the tin ions neighboring the defect, consistent with reduction. In addition, a polarization of the charge on the oxygen ions surrounding the defect can be seen. The charge density for the defect state 0.3 eV below the CBM is shown in Figure 8c and shows the density to be mainly on O ions near the defect with some lone-pair-like density on the neighboring Sn ions. Similar hybridization of Sn 5s with O 2p states has been observed previously for lone pairs in SnO.[40,41]

Electronic Structure of O-Rich Defects: Oxygen Interstitials

At high oxygen partial pressure, $O_i'' + 2h^{\bullet}$ has the lowest defect energy and hence will dominate the defect structure. Isolated O_i'' defects, inserted into tetrahedral and octahedral sites, both relaxed to give the same structure (Figure 9b) which is the reason for the equal energies observed in Table 2. However, instead of the expected O^{2-} interstitial (O_i''), the inserted oxygen relaxes toward a lattice oxygen to form a peroxide anion (O_2^{2-}) substituting at a lattice site similar to that observed in calculations in ZnO.[51] The Bader charges (Table 6) show each peroxide oxygen to be in a −1 charge state with a bond length typical of a peroxide ion. The remaining −2 charge results in a tin reduction which is delocalized over all tin atoms as seen by the 1.49*e* difference in total Sn charge between the nondefective and defective cells. The inserted O_i'' thus relaxes to give $(O_2)_O^{\times} + Sn_{Sn}''$.

The insertion of a $O_i'' + 2h^{\bullet}$ defect cluster also results in the formation of a peroxide ion ($(O_2)_O^{\times}$). The apparent high binding energy in Table 2 occurs as the isolated formation energy is for O_i'' compensated by two oxygen holes. As O_i'' is actually composed of $(O_2)_O^{\times}$ charge compensated by a tin reduction, the tin reduction and the oxygen holes charge annihilate in the defect cluster, resulting in a significantly lower defect energy compared to the isolated defect with the average Sn charge remaining similar to pure SnO_2. This illustrates the importance of considering defect structure as well as energetics. Two slightly different structures were obtained depending on whether the interstitial was inserted into a tetrahedral or octahedral lattice site. The octahedral interstitial relaxed to give the structure shown in Figure 9a in which one peroxide oxygen bonded to two tin atoms with bond lengths of 2.07 Å, while the second bonds to one tin atom with a bond length of 2.03 Å. A lower energy structure was obtained when the interstitial was inserted into a tetrahedral lattice site. Each peroxide oxygen bonds to two tin atoms with bond lengths of 2.24 Å and 2.06 Å (Figure 9b).

The EDOS for both structures is shown in Figure 10 with the VBM at 0 eV. Both structures show an unoccupied state of O 2p character from the peroxide ion located at 4.9 eV for

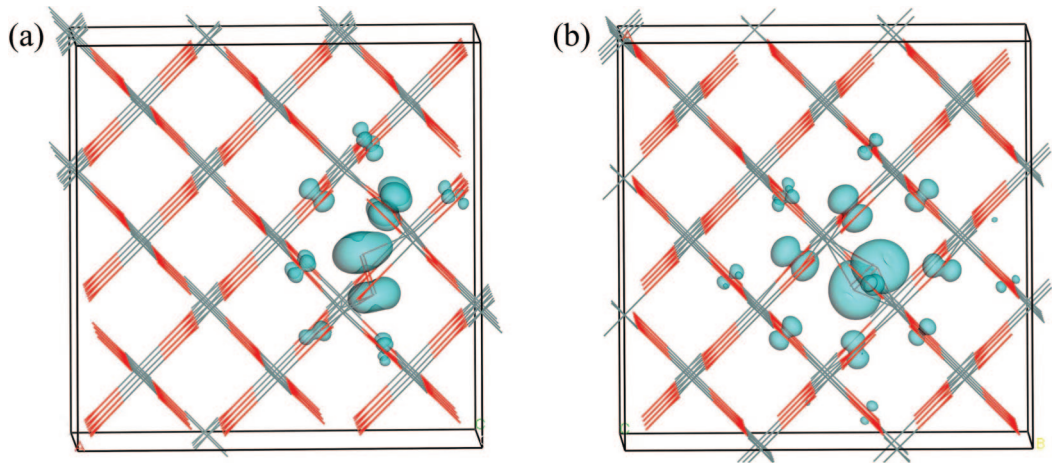

Figure 11. Partial charge density plots of (a) defect state at −0.4 eV for $(O_2)_O^{\times}$−oct at isosurface level of 0.05 e/Å^3; (b) defect state at −0.2 eV of $(O_2)_O^{\times}$−tet at isosurface level of 0.05 e/Å^3.

$(O_2)_O^x$−oct and 4.4 eV for $(O_2)_O^x$−tet and is associated with an empty σ^* level of the peroxide ion. As these states occur deep into the conduction band, p-type conductivity through oxygen holes is prohibitive. Both structures show a localized state at the top of the valence band of O 2p character from the peroxide ion. It appears to be more localized in the tetrahedral structure than in the octahedral geometry. The partial charge density for this state (Figure 11) shows it to be associated mainly with the oxygen atoms of the peroxide ion with small contributions from oxygen ions surrounding the defect suggesting it to be a filled π^* level for the peroxide ion.

Discussion and Conclusions

Previous DFT studies have focused on defect energetics, with a lack of detailed geometric and electronic structure analysis.[26,27] From a comprehensive examination of the defect structure we have shown that in many cases, the inserted defect relaxes to give a completely different defect. For example, tin interstitials inserted into tetrahedral sites relax to give split interstitial structures, while for oxygen interstitials the inserted defect relaxes to give a substitutional peroxide ion. This emphasizes the importance of careful consideration of the defect structure as well as the energetics.

The severe underestimation of the band gap which is inherent to GGA-DFT calculations can introduce large quantitative errors in the formation energies (in particular for donor defects). Although it is possible to account for these errors through the application of an a posteriori correction,[52] we do not follow this route due to the arbitrary nature of the corrections and the serious approximations involved. However, the results are still qualitatively correct and in future studies we aim to employ DFT with Fock exchange (hybrid-DFT), which should give a better description of the band gap so that we can gain a more comprehensive understanding of the electronic structure of tin dioxide.

Our analysis shows that nonstoichiometric defects are far more likely to occur than stoichiometric defects, which is the reason for the observed nonstoichiometry of SnO_2. Oxygen deficiency ($SnO_{2-\delta}$) occurs due to the presence of $V_O^{\bullet\bullet}$ with charge compensation via Sn_{Sn}'' giving rise to n-type conductivity. However, varying the oxygen partial pressure will affect the stability of this defect and under extreme oxygen-rich conditions, oxygen excess ($SnO_{2+\delta}$) will occur due to the presence of peroxide ions ($(O_2)_O^x$). The formation of this defect is unlikely to lead to intrinsic p-type conductivity as it is charge neutral and does not produce any free hole carriers in the valence band. The existence of peroxide ions in tin dioxide has already been proposed in heavily doped SnO_2 when the introduction of substitutional M^{3+} ions leads to the formation of localized oxygen holes.[53] Instead of acting as charge carriers, adjacent holes tend to pair up to form peroxide ions which act as charge traps. At high oxygen partial pressure, the only defect that could induce p-type behavior is $V_{Sn}'''' + 4h^{\bullet}$ which has a higher formation energy than $V_O^{\bullet\bullet}$ so that even under oxygen-rich conditions, n-type conductivity will dominate.

We have shown that the stability of $V_O^{\bullet\bullet} + Sn_{Sn}''$ is due to the loss in coordination of tin ions neighboring the vacancy, making them more susceptible to Sn(II) reduction. However, we do not observe a highly localized reduction to a single Sn(II) species. Instead, we observe a delocalized reduction over all tin ions in the system with a partial localization on the three tin ions neighboring the vacancy. The failure to observe a single Sn^{2+} ion may be related to the self-interaction error inherent in DFT.[48] We have confirmed the existence of shallow donor levels at the bottom of the conduction band for $V_O^{\bullet\bullet} + Sn_{Sn}''$, which have been observed experimentally.[16,22] Conductivity is likely to occur due to ionization of these levels, with the mobility of electrons from Sn(II) to Sn(IV) sites. We have determined these levels to be a mixture of Sn 5s and O 2p character from tin and oxygen ions neighboring the vacancy. The hybridization of these states is not unexpected as previous calculations for SnO have observed the hybridization of lone pair states for Sn(II).[40,41]

Acknowledgment. This material is based upon works partially supported by the Science Foundation Ireland under Grant No. [06/IN.1/I92] and an IRCSET postgraduate studentship award. We also acknowledge the HEA and NDP for the PRTLI programs IITAC and e-INIS, and Trinity Centre for High Performance Computing for access to the TCHPC computational facilities.

References and Notes

(1) Ingram, B. J.; Gonzalez, G. B.; Kammler, D. R.; Bertoni, M. I.; Mason, T. O. *J. Electroceram.* **2004**, *13*, 167–175.
(2) Hosono, H. *Thin Solid Films* **2007**, *515*, 6000–6014.
(3) Godinho, K. G.; Watson, G. W.; Walsh, A.; Green, A. J. H.; Payne, D. J.; Harmer, J.; Egdell, R. G. *J. Mater. Chem.* **2008**, *18*, 2798.
(4) Minami, T. *Semicond. Sci. Technol.* **2005**, *20*, S35–S44.
(5) Yamanaka, T.; Kurashima, R.; Mimaki, J. *Z. Kristallogr.* **2000**, *215*, 424–428.
(6) Watson, G. W. *J. Chem. Phys.* **2001**, *114*, 758–763.
(7) Barbarat, P.; Matar, S. F.; LeBlevennec, G. *J. Mater. Chem.* **1997**, *7*, 2547–2550.
(8) Calatayud, M.; Andres, J.; Beltran, A. *Surf. Sci.* **1999**, *430*, 213–222.
(9) Errico, L. A. *Physica B* **2007**, *389*, 140–144.
(10) Maki-Jaskari, M. A.; Rantala, T. T. *Phys. Rev. B* **2001**, *64*, 075407.
(11) Robertson, J.; Xiong, K.; Clark, S. J. *Thin Solid Films* **2006**, *496*, 1–7.
(12) Maestre, D.; Ramirez-Castellanos, J.; Hidalgo, P.; Cremades, A.; Gonzalez-Calbet, J. M.; Piqueras, J. *Eur. J. Inorg. Chem.* **2007**, 1544–1548.
(13) Ming, F.; Xiaoli, T.; Xueli, C.; Lide, Z.; Peisheng, L.; Zhi, J. *J. Phys. D: Appl. Phys.* **2007**, *40*, 7648–7651.
(14) Vincent, C. A. *J. Electrochem. Soc.* **1972**, *119*, 515–521.
(15) Alterkop, B.; Parkansky, N.; Goldsmith, S.; Boxman, R. L. *J. Phys. D* **2003**, *36*, 552–558.
(16) Samson, S.; Fonstad, C. G. *J. Appl. Phys.* **1973**, *44*, 4618–4621.
(17) Maier, J.; Gopel, W. *J. Solid State Chem.* **1988**, *72*, 293–302.
(18) Dinola, P.; Morazzoni, F.; Scotti, R.; Narducci, D. *J. Chem. Soc., Faraday Trans.* **1993**, *89*, 3711–3713.
(19) Morazzoni, F.; Canevali, C.; Chiodini, N.; Mari, C.; Ruffo, R.; Scotti, R.; Armelao, L.; Tondello, E.; Depero, L.; Bontempi, E. *Mater. Sci. Eng., C* **2001**, *15*, 167–169.
(20) Sun, S. H.; Meng, G. W.; Zhang, G. X.; Gao, T.; Geng, B. Y.; Zhang, L. D.; Zuo, J. *Chem. Phys. Lett.* **2003**, *376*, 103–107.
(21) Ningthoujam, R.; Lahiri, D.; Sudarsan, V.; Poswal, H. K.; Kulshreshtha, S. K.; Sharma, S. M.; Bhushan, B.; Sastry, M. D. *Mater. Res. Bull.* **2007**, *42*, 1293–1300.
(22) Prades, J. D.; Arbiol, J.; Cirera, A.; Morante, J. R.; Avella, M.; Zanotti, L.; Comini, E.; Faglia, G.; Sberveglieri, G. *Sensor Actuat. B* **2007**, *126*, 6–12.
(23) Freeman, C. M.; Catlow, C. R. A. *J. Solid State Chem.* **1990**, *85*, 65–75.
(24) Hines, R. I.; Allan, N. L.; Flavell, W. R. *J. Chem. Soc., Faraday Trans.* **1996**, *92*, 2057–2063.
(25) Robertson, J. *Phys. Rev. B* **1984**, *30*, 3520–3522.
(26) Kilic, C.; Zunger, A. *Phys. Rev. Lett.* **2002**, *88*, 095501.
(27) Singh, A. K.; Janotti, A.; Scheffler, M.; Van de Walle, C. G. *Phys. Rev. Lett.* **2008**, 055502.
(28) Kresse, G.; Hafner, J. *Phys. Rev. B* **1994**, *49*, 14251–14269.
(29) Kresse, G.; Furthmuller, J. *Comput. Mater. Sci.* **1996**, *6*, 15–50.
(30) Kohn, W.; Sham, L. J. *Phys. Rev.* **1965**, *140*, 1133.
(31) Perdew, J. P.; Burke, K.; Ernzerhof, M. *Phys. Rev. Lett.* **1996**, *77*, 3865–3868.
(32) Blochl, P. E. *Phys. Rev. B* **1994**, *50*, 17953–17979.
(33) Monkhorst, H. J.; Pack, J. D. *Phys. Rev. B* **1976**, *13*, 5188.
(34) Curtiss, L. A.; Raghavachari, K.; Redfern, P. *J. Chem. Phys.* **1997**, *106*, 1063–1079.
(35) *CRC Handbook of Chemistry and Physics*, 88th ed.; Lide, D. R., Ed.; CRC Press: Boca Raton, FL, 2008.

(36) Murnaghan, F. D. *Proc. Natl. Acad. Sci. U.S.A.* **1944**, *30*, 244–247.
(37) Sanville, E.; Kenny, S. D.; Smith, R.; Henkelman, G. *J. Comput. Chem.* **2007**, *28*, 899–908.
(38) Mimaki, J.; Tsuchiya, T.; Yamanaka, T. *Z. Kristallogr.* **2000**, *215*, 419–423.
(39) Moreno, M. S.; Egerton, R. F.; Rehr, J. J.; Midgley, P. A. *Phys. Rev. B* **2005**, *71*, 035103.
(40) Walsh, A.; Watson, G. W. *Phys. Rev. B* **2004**, *70*, 235114.
(41) Walsh, A.; Watson, G. W. *J. Phys. Chem. B* **2005**, *109*, 18868–18875.
(42) Zhu, Y. Z.; Chen, G. D.; Ye, H.; Walsh, A.; Moon, C. Y.; Wei, S.-H. *Phys. Rev. B* **2008**, *77*, 245209.
(43) Nagasawa, M.; Shionoya, S. *Phys. Rev. Lett.* **1968**, *21*, 1070.
(44) Mryasov, O. N.; Freeman, A. J. *Phys. Rev. B* **2001**, *64*, 233111.
(45) Sensato, F. R.; Filho, O. T.; Longo, E.; Sambrano, J. R.; Andres, J. *J. Mol. Struc.-Theochem* **2001**, *541*, 69–79.
(46) McGuinness, C.; Stagarescu, C. B.; Ryan, P. J.; Downes, J. E.; Fu, D. F.; Smith, K. E.; Egdell, R. G. *Phys. Rev. B* **2003**, *68*, 165104.
(47) Themlin, J. M.; Sporken, R.; Darville, J.; Caudano, R.; Gilles, J. M.; Johnson, R. L. *Phys. Rev. B* **1990**, *42*, 11914–11925.
(48) Nolan, M.; Grigoleit, S.; Sayle, D. C.; Parker, S. C.; Watson, G. W. *Surf. Sci.* **2005**, *576*, 217–229.
(49) Morgan, B. J.; Watson, G. W. *Surf. Sci.* **2007**, *601*, 5034–5041.
(50) Scanlon, D. O.; Walsh, A.; Morgan, B. J.; Nolan, M.; Fearon, J.; Watson, G. W. *J. Phys. Chem. C* **2007**, *111*, 7971–7979.
(51) Sokol, A. A.; French, S. A.; Bromley, S. T.; Catlow, C. R. A.; van Dam, H. J. J.; Sherwood, P. *Faraday Discuss.* **2007**, *134*, 267–282.
(52) Zhang, S. B.; Wei, S.-H.; Zunger, A. *Phys. Rev. B* **2001**, *63*, 075205.
(53) Fitzgerald, C. B.; Venkatesan, M.; Dorneles, L. S.; Gunning, R.; Stamenov, P.; Coey, J. M. D.; Stampe, P. A.; Kennedy, R. J.; Moreira, E. C.; Sias, U. S. *Phys. Rev. B* **2006**, *74*, 115307.

JP807753T